catalysts

MDPI

Article

Improvement in the Photocatalytic Hydrogen Production of Flower-Shaped $ZnIn_2S_4$ by Surface Modification with Amino Silane

Xiangyu Chen, Benliang Liang * and Luting Yan *

Department of Materials, School of Physical Science and Engineering, Beijing Jiaotong University, Beijing 100044, China; 21271004@bjtu.edu.cn

* Correspondence: blliang@bjtu.edu.cn (B.L.); ltyan@bjtu.edu.cn (L.Y.)

Abstract: $ZnIn_2S_4$ has attracted extensive attention in the field of photocatalytic hydrogen production because of its suitable band gap and excellent photoelectrochemical properties. However, its lower photogenerated carrier separation efficiency and high degree of photocorrosion severely restricts its photocatalytic activity. In this work, the photocatalytic hydrogen production performance of $ZnIn_2S_4$ modified with 3-aminopropylmethoxysilane was studied. Surface modification by amino silane not only regulated the band gap and enhanced the light absorption of $ZnIn_2S_4$ but it also increased the colloidal stability of the $ZnIn_2S_4$ suspension and enhanced the adsorption of H^+ on the active surface sites, thereby improving the photocatalytic hydrogen production performance. Compared with that of unmodified $ZnIn_2S_4$, the photocatalytic hydrogen production rate of surface-modified $ZnIn_2S_4$ increased by 1.46 times, and after four cycles for 12 h, the hydrogen production efficiency remained at 75.14%.

Keywords: hydrogen production; photocatalysis; $ZnIn_2S_4$; surface modification

Citation: Chen, X.; Liang, B.; Yan, L. Improvement in the Photocatalytic Hydrogen Production of Flower-Shaped $ZnIn_2S_4$ by Surface Modification with Amino Silane. *Catalysts* **2024**, *14*, 607. https://doi.org/10.3390/catal14090607

Academic Editor: Jorge Bedia

Received: 31 July 2024
Revised: 4 September 2024
Accepted: 5 September 2024
Published: 10 September 2024

1. Introduction

Photocatalytic hydrogen production is a key research direction for future hydrogen energy generation, and the development of efficient photocatalysts is crucial to improving photocatalytic performance [1,2]. During the past few decades, tremendous efforts have been devoted to developing nontoxic, low-cost, efficient, and stable photocatalysts for water splitting, including metal oxides, sulfides, and nitrides with different structures and compositions [3–6]. To further improve the performance of semiconductors in photocatalytic hydrogen production, it is necessary not only to broaden the photoresponse range and enhance the absorption efficiency of semiconductors but also to improve the separation efficiency of photogenerated electron–hole pairs. The common techniques used include precious metal nanoparticle deposition [7–9], elemental doping [10–12], defect structure [13–15], heterojunctions with other semiconductors [16,17], surface modification [18,19], and composite nanostructures [20,21]. However, these strategies generally involve complex sample preparation procedures and harsh reaction conditions, which are not conducive to reducing the manufacturing cost of photocatalysts.

Owing to the effective separation and migration of photogenerated electrons and holes to different surface regions, the formation of redox-active sites, and the triggering of photocatalytic reactions, the surface characteristics of semiconductors significantly affect their photocatalytic activities. Additionally, surface modification can design functional groups on the surface of photocatalysts through covalent bonding, becoming a simple and low-energy method for regulating photocatalysts. Hu et al. [22] prepared ethylenediamine-modified TiO_2, which exhibited an excellent photocatalytic hydrogen evolution rate through synchronously broadening the light absorption and increasing the conduction band position

of TiO_2. Wanag et al. [23] reported that APTES modification of TiO_2 improved the photocatalytic decomposition of methylene blue. Lei et al. [24] studied the interfacial molecular regulation of TiO_2 for enhanced photocatalytic hydrogen production. The electron-donating properties of the amine group modulated both the band gap and carrier separation efficiency of TiO_2, leading to a 12-fold increase in photocatalytic hydrogen production. Shao et al. [25] applied poly(3-hexylthiophene) to modify black phosphorus (BP), and the formed built-in electric field promoted the enrichment of photogenerated electrons on the BP surface, which greatly enhanced the photocatalytic activity.

$ZnIn_2S_4$ (ZIS) has attracted great interest because of its suitable band gap, good chemical stability, simple and flexible preparation methods, and excellent light absorption. However, as a photocatalyst, its lower photogenerated carrier separation and migration efficiency, sluggish surface reaction kinetics, and high degree of photocorrosion severely restricts its photocatalytic activity [26–28]. Therefore, several strategies have been used to improve the photocatalytic performance of $ZnIn_2S_4$, such as morphology regulation, vacancy engineering, compounding with semiconductors, element doping, and the construction of heterojunctions [29–32]. Among them, constructing heterojunctions can effectively enhance the separation of photogenerated carriers and suppress photocorrosion. The use of multidimensional hierarchical hollow $Co_3O_4/ZnIn_2S_4$ tubular core–shell heterostructures resulted in a photocatalytic hydrogen production rate of 3844.12 $\mu mol \cdot g^{-1} \cdot h^{-1}$, which is 4.67 times greater than that achieved with pure $ZnIn_2S_4$ [33]. The ZIS-PyP S-scheme photocatalyst has a photocatalytic H_2 evolution rate of 54 $\mu mol \cdot h^{-1}$, which is 2.5-fold greater than that of pure $ZnIn_2S_4$ [34]. However, the formation of high-quality heterojunctions requires precise control of the interfaces and optimization of the band alignment. In addition, there is still controversy over the migration direction of photogenerated carriers in direct Z-scheme heterojunctions [35]. Compared with constructing heterojunctions, surface modification with organic small molecules is relatively simpler and more effective. Herein, $ZnIn_2S_4$ was synthesized via a hydrothermal reaction method, followed by surface modification with 3-aminopropylmethoxysilane (APS). The purpose of surface modification is as follows: first, the band gap of $ZnIn_2S_4$ is regulated through the participation of electron-donating amino groups of APS, increasing light absorption and accelerating the separation and migration of photogenerated carriers; second, the colloidal stability of the $ZnIn_2S_4$ suspension through the spatial hindrance provided by APS, along with the increased adsorption of H^+ by amino groups, synergistically improves the photocatalytic hydrogen production rate of $ZnIn_2S_4$.

2. Results

2.1. Morphology and Structure

The ZIS and surface-modified ZIS were characterized via XRD, and the corresponding results are shown in Figure 1a. Pure ZIS had characteristic diffraction peaks at 21.6°, 27.7°, 47.2°, and 52.4°, corresponding to the (006), (102), (110), and (116) crystal planes of hexagonal ZIS (JCPDS#72-0773), respectively. No significant changes in the crystalline structure of the surface-modified ZIS were observed, and APS modification did not contribute to phase transformation. The XRD patterns of ZIS-APS were essentially consistent with those of pure ZIS. Figure 1b shows the FTIR spectra of ZIS and ZIS-APS. In addition to the broad absorption bands at 3300–3500 cm^{-1}, 1600–1650 cm^{-1}, and 1396 cm^{-1}, which corresponded to typical H–O–H, O–H, and C–O stretching vibrations of the absorbed H_2O and atmospheric CO_2, no particular functional groups existed on the ZIS surface [36,37]. During the surface modification process, silane was first hydrolyzed into silanol and then condensed with the –OH groups on the ZIS surface. $–NH_2$ stretching vibrations had two absorption peaks at 3400–3490 cm^{-1}. The peaks at 2900–3000 cm^{-1} were attributable to symmetric and asymmetric $–CH_2$ stretching in the alkyl chain introduced by silane. The peak at approximately 1600 cm^{-1} could be assigned to the N–H bending vibrations of primary amines, the peak near 1450 cm^{-1} belonged to the in-plane bending vibration of C–H, and the peak located at 1380 cm^{-1} belonged to the C–N bands. The peak corresponding to

Si–O–Si was found at 1160 cm^{-1}, indicating self-condensation among the silanol groups. The FTIR spectra indicated the successful modification of ZIS by amino silane.

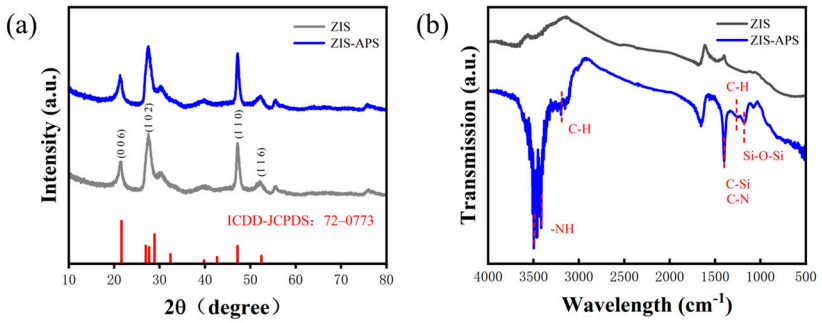

Figure 1. XRD patterns of ZIS and ZIS-APS (**a**) and FTIR spectra of ZIS and ZIS-APS (**b**).

TEM (Figure 2a), SEM (Figure 2b,c), and EDS layered images confirmed the morphology and structure of ZIS and ZIS-APS. These results indicated that ZIS consisted of flower-shaped microspheres composed of many nanoflakes with diameters of approximately 1–2 μm. The flower-shaped microsphere structure has a larger specific surface area and more reactive sites, which is conducive to photocatalytic reactions. The EDS results revealed that the surface morphological structure of the amine-based APS modification was uniform. The images show that the obtained sample contained N, Si, S, Zn, and In. Both Si and N were homogeneously dispersed throughout the surface, indicating that the silane APS agent was modified onto the ZIS.

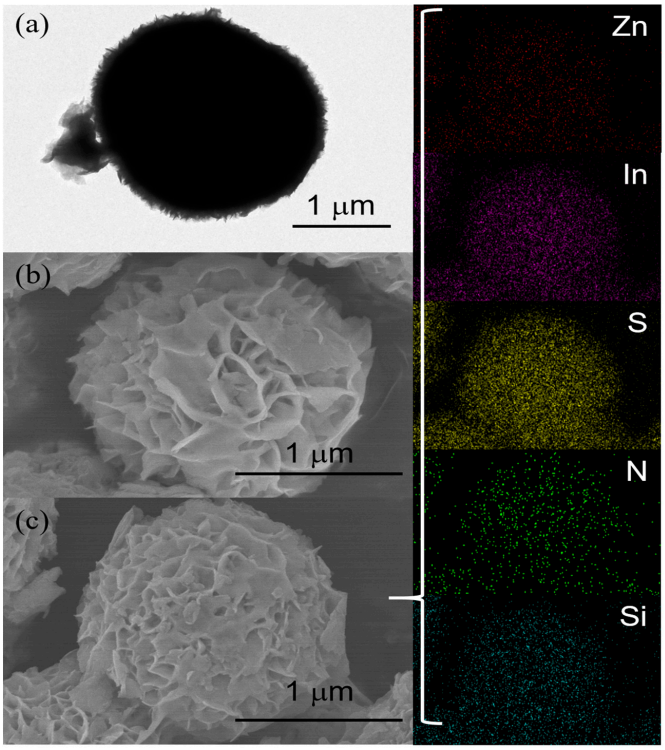

Figure 2. TEM image of ZIS (**a**), SEM images of ZIS (**b**), and SEM images of ZIS-APS (**c**).

The surface composition and element valence states were further investigated via XPS (Figure 3). XPS survey scans (Figure 3a) revealed that In, S, Zn, N, Si, O, and C coexisted in the samples. Figure 3e–g show the specific XPS spectra of Zn 2p, In 3d, and S 2p for the prepared $ZnIn_2S_4$ and modified $ZnIn_2S_4$. The difference in binding energies between Zn $2p_{1/2}$ and $2p_{3/2}$ was approximately 23.1 eV, suggesting a typical Zn^{2+} in $ZnIn_2S_4$ [38,39].

The In 3d spectrum exhibited two peaks at 445.1 eV and 452.6 eV, which were attributed to the In $3d_{5/2}$ and In $3d_{3/2}$ energy levels, respectively. The S 2p peaks were located at 161.85 eV and 163.05 eV, corresponding to S $2p_{3/2}$ and S $2p_{1/2}$, respectively. The above XPS binding energies confirmed that the chemical valence states of In and S were In^{3+} and S^{2-}. Affected by APS bonding, the Zn 2p, In 3d, and S 2p peaks in ZIS-APS shifted in the lower energy direction. The Si 2p peak in Figure 3c and the significantly enhanced C 1 s peak in Figure 3d further demonstrated the introduction of APS. The two N 1 s peaks at 399.7 and 401.7 eV (Figure 3b) were found in the high-resolution N 1 s spectrum, corresponding to the N–H orbitals of the primary amine and protonated amine NH_3^+, respectively. This indicates that the amine groups introduced by silane surface modification enhanced the adsorption of H^+ in water, which is beneficial for improving the photocatalytic performance. The above results are consistent with the previous SEM and FTIR results, indicating the successful modification of ZIS with APS.

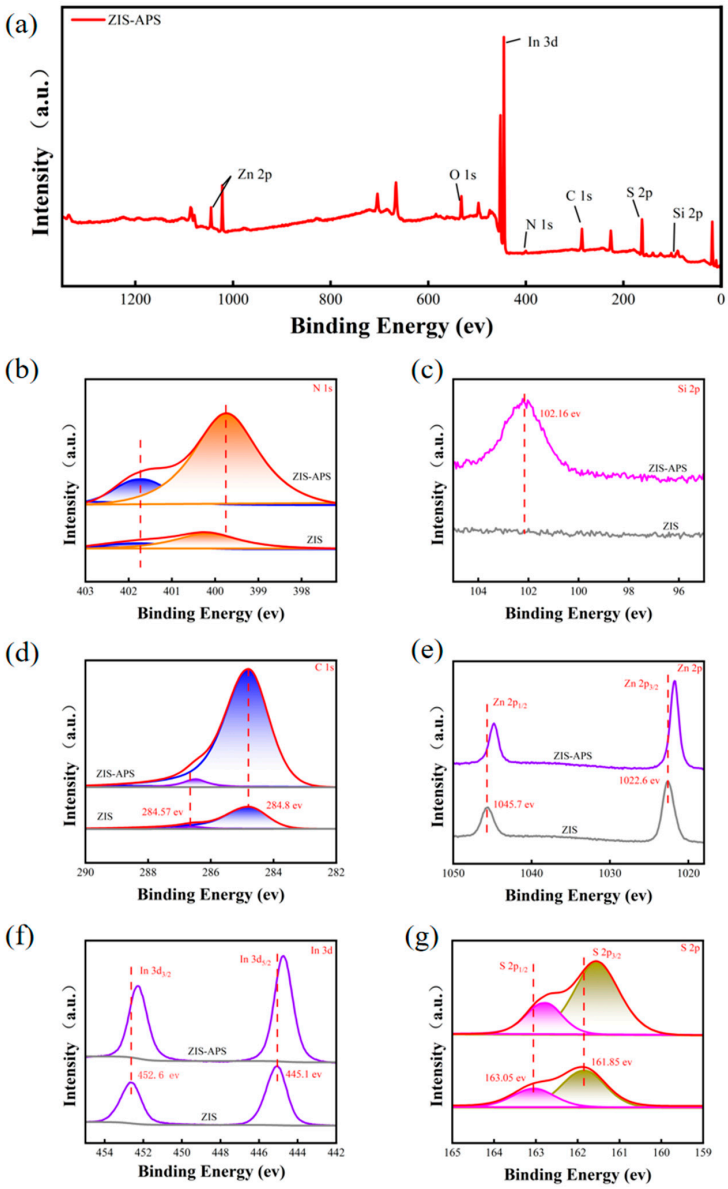

Figure 3. XPS spectra of ZIS and modified ZIS: (**a**) survey of ZIS-APS, (**b**) N 1s, (**c**) Si 2p, (**d**) C 1s, (**e**) Zn 2p, (**f**) In 3d and (**g**) S 2p.

2.2. Optical Properties and Band Gap

As depicted in Figure 4a,b, the absorption properties and band gaps of ZIS and ZIS-APS were studied via UV–vis diffuse reflection spectroscopy. Pure $ZnIn_2S_4$ had high absorbance, with an absorption edge at approximately 480 nm. Compared with that of pure ZIS, the absorption performance of ZIS-APS was significantly greater in the wavelength range of 300–800 nm. Furthermore, the band gaps of ZIS and ZIS-APS were calculated according to the classical Tauc plot calculation method. The band gap energy of ZIS was 2.38 eV, whereas the band gap energy of amine-functionalized ZIS was reduced to 2.35 eV. The MS curves in Figure 4c exhibited a positive slope, indicating that ZIS is an n-type semiconductor. The inset in Figure 4c shows that the flat band potential is relatively stable at different frequencies. The flat band potentials of ZIS and ZIS-APS were −1.04 and −1.20 eV, respectively. On the basis of the Tauc plot and MS results, the energy band structures of ZIS and ZIS-APS are listed in Figure 4d. Compared with that of pristine ZIS, the conduction band position of ZIS-APS was negatively shifted by 0.16 eV, indicating an enhanced H^+ reduction ability.

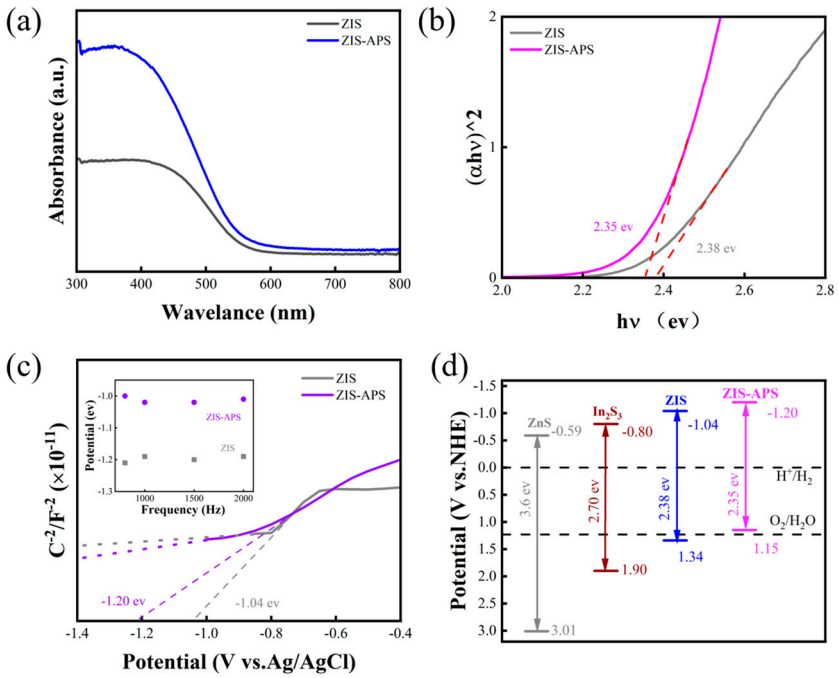

Figure 4. Optical properties of ZIS and ZIS-APS. UV–vis DRS spectra (**a**), Tauc energy band gap (**b**), MS plots, the inset shows the flat band potential at different frequencies (**c**) and band structure alignments (**d**). The band potentials for In_2S_3 and ZnS were obtained from Refs. [40,41].

2.3. Photocatalytic H_2 Evolution

Xenon lamps provide simulated natural light illumination, and photocatalytic hydrogen production testing was conducted by combining a photocatalytic cycling instrument with gas chromatography. The changes in photocatalytic hydrogen evolution over time for ZIS and ZIS-APS are shown in Figure 5. The amount of hydrogen produced increased linearly with time, and the hydrogen production rates of the amine-modified ZIS were substantially greater than those of pure ZIS. Pure ZIS exhibited a photocatalytic hydrogen production rate of 3.51 mmol·g^{-1}·h^{-1}, whereas the rate of H_2 evolution of ZIS-APS reached 5.13 mmol·g^{-1}·h^{-1}, which was 1.46 times greater than that of pure ZIS. The cyclic test results in Figure 5c show that the ZIS-APS photocatalyst maintained a relatively stable hydrogen production ability without any substantial decrease after four cycles for 12 h, with a 75.14% initial hydrogen production rate. ZIS had a lower hydrogen production rate in the first round, reached its peak in the second round, and then decreased. However, the

hydrogen production rate remained lower than that of ZIS-APS throughout the four rounds. Compared with data reported in other studies (Figure 5d, some of the data were obtained under visible light), the hydrogen production rate of ZIS-APS was further ahead, and it had excellent stability.

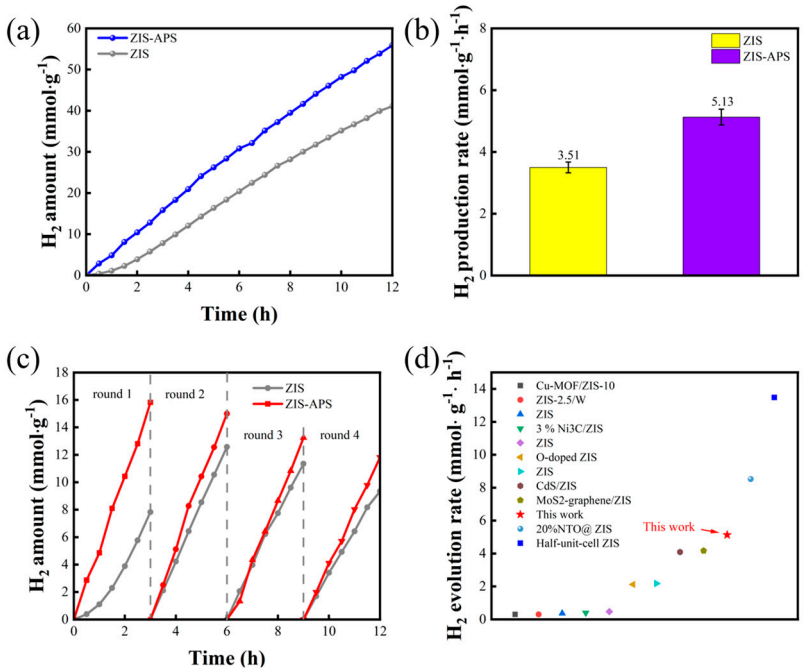

Figure 5. Hydrogen production curves (**a**), comparison of average hydrogen production rates (**b**), cyclic tests (**c**), and comparison of hydrogen production rates with data reported in other studies [28,31,42–48] (**d**).

3. Discussion

To further explore the carrier separation and migration efficiency, the photocurrent and electrochemical impedance spectroscopy (EIS) results of ZIS and ZIS-APS were obtained via an electrochemical workstation, and the results are shown in Figure 6. Figure 6a shows the time-dependent photocurrent measurements. ZIS-APS exhibited a higher photocurrent density that correlated well with the on/off cycle of simulated sunlight, indicating that the covalently modified amino molecules increased light absorption and facilitated efficient electron–hole pair separation. The facilitated charge transfer of ZIS-APS was further confirmed by EIS (Figure 6b). Compared with pure ZIS, ZIS-APS had a smaller arc radius (the Rct values of ZIS and ZIS-APS were 10 Ω and 0.84 Ω, respectively), which indicates that surface modification of ZIS with amino silane can substantially accelerate the charge transfer of ZIS. These electron transfers generally help separate photogenerated electron–hole pairs and consequently result in higher catalytic performance than that of pure $ZnIn_2S_4$.

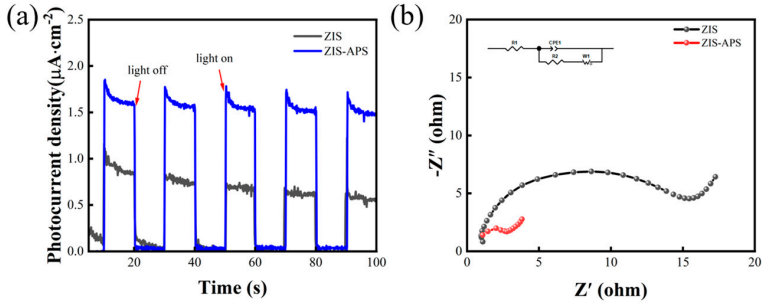

Figure 6. Photocurrent curves (**a**) and impedance diagram (**b**).

Figure 7 shows a schematic diagram of the increased photocatalytic hydrogen production mechanism. During the surface modification process, silane is first hydrolyzed into silanol and then condensed with the –OH groups on the ZIS surface. First, the long-chain alkyl groups introduced by surface modification enhance the colloidal stability of the ZIS suspension. Second, electron-donating amino groups participate in band gap regulation, improving light absorption and promoting the migration and separation of photogenerated carriers. Furthermore, the $–NH_2$ groups on the surface of ZIS are positively charged owing to protonation, which promotes the adsorption of H^+ on the ZIS surface. Therefore, the photocatalytic performance and stability of $ZnIn_2S_4$ were significantly improved. This is consistent with the previous UV–vis absorption, photocurrent, and impedance results.

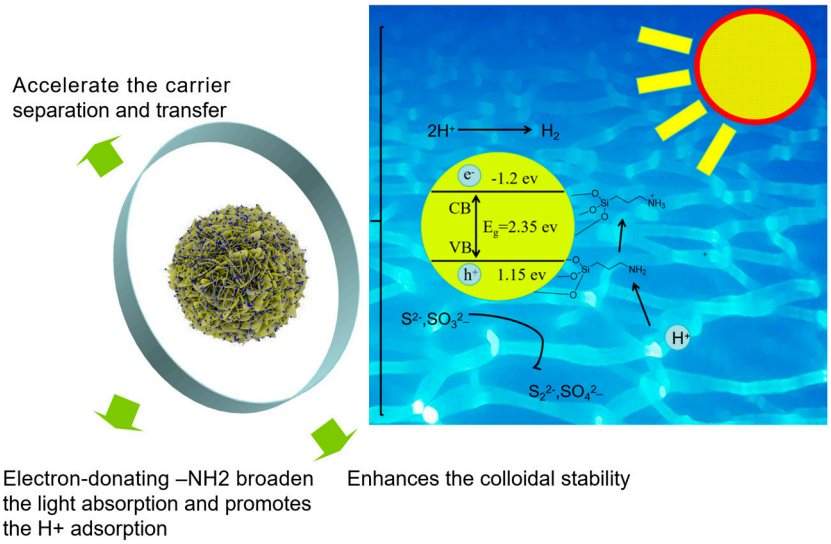

Figure 7. Schematic diagram of the photocatalytic hydrogen production mechanism.

4. Materials and Methods

Materials. Zinc chloride ($ZnCl_2$), indium trichloride tetrahydrate ($InCl_3 \cdot 4H_2O$), and thioacetamide (C_2H_5NS, TAA) were obtained from Beijing Inno-chem Technology Co., Ltd., Beijing, China, 3-aminopropylmethoxysilane (APS) was purchased from Acros. Sodium sulfite nonahydrate ($Na_2S \cdot 9H_2O$) and sodium sulfite (Na_2SO_3) were purchased from Tianjin Fuchen Chemical Reagent Factory. All chemicals were used without further purification.

Preparation of $ZnIn_2S_4$. $ZnIn_2S_4$ was prepared via hydrothermal methods. First, 1 mmol of $ZnCl_2$, 2 mmol of $InCl_3 \cdot 4H_2O$, and 4 mmol of TAA were dissolved in 80 mL of deionized water. After stirring for 30 min, the mixture was transferred to a 100 mL Teflon-lined stainless-steel autoclave and maintained at 80 °C for 12 h. The resulting powder was separated at 5000 rpm and then washed once with deionized water and 2× with ethanol to remove any residual chemicals. Finally, the powder was dried at 60 °C for 12 h. The obtained $ZnIn_2S_4$ was denoted ZIS.

Surface modification of $ZnIn_2S_4$. Two hundred milligrams of $ZnIn_2S_4$ was dispersed in 100 mL of ethanol with a 1.5 wt% concentration of APS at room temperature for 24 h. The powder was obtained after centrifugation and rinsed with distilled water and ethanol to remove residual chemicals. Finally, the obtained powder was dried at 60 °C for 12 h. The modified $ZnIn_2S_4$ was denoted ZIS-AP. Figure 8 shows a schematic diagram of the preparation process of ZIS and ZIS-APS.

Characterization. The morphology and microstructure of the obtained products were observed by scanning electron microscopy (SEM, Hitachi S4800, Hitachi Ltd., Tokyo, Japan) and transmission electron microscopy (TEM, Tecnai G2F30 S-TWIN, FEI, Atlanta, GA, USA). The phase structures were studied via X-ray diffractometry (XRD, Ultima IV, Rigaku, Tokyo, Japan). The surface elemental compositions were analyzed through X-ray photoelectron spectroscopy (XPS, Axis Supra, Kratos Analytical Ltd., Manchester, UK). The Tauc plots of

the composite were constructed on the basis of UV–visible diffuse reflectance spectroscopy (DRS Cary 5000, Agilent Technologies Inc, Santa Clara, CA, USA). By combining the Mott–Schottky (MS) plot with the Tauc plot, the changes in the positions of the valence band and conduction band of the samples were determined. The photocurrent and electrochemical impedance spectroscopy (EIS) results were measured with a CHI760E workstation (Shanghai Chenhua, Shanghai, China) to explore the charge separation efficiency and transport capability of the photocatalyst.

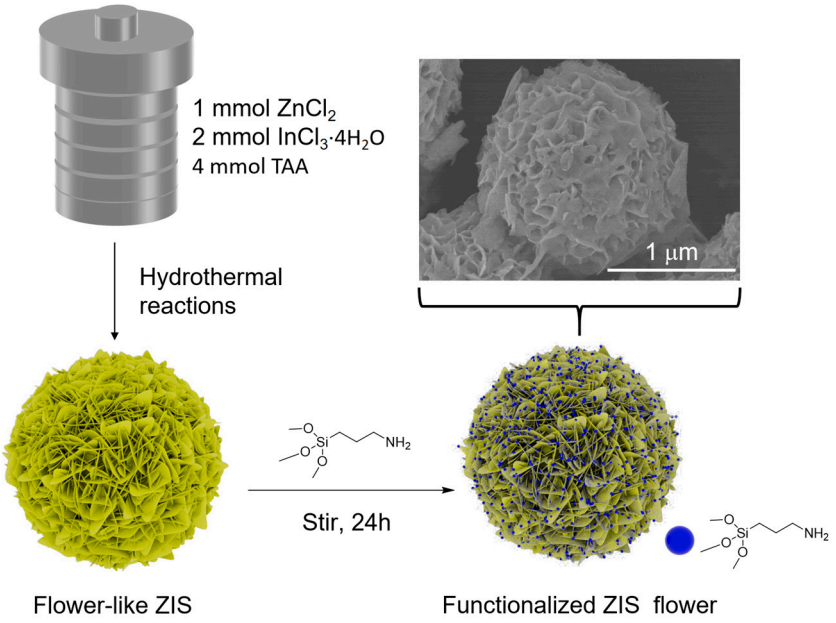

Figure 8. Schematic diagram of the preparation process of ZIS and ZIS-APS (Blue ball represents silane).

Photocatalytic H_2 production test. The photocatalytic activity of the catalyst was assessed in a 200 mL sealed quartz reactor under 300 W xenon lamp irradiation. A total of 10 mg of catalyst was added to a reactor containing 100 mL of a mixed solution containing 0.25 mol·L^{-1} Na_2SO_3 and 0.35 mol·L^{-1} Na_2S. The reaction temperature was controlled at 20 °C by circulating cooling water, and N_2 purging was maintained for 30 min to remove residual air. The generated hydrogen was detected via a gas chromatograph equipped with a TCD detector.

5. Conclusions

In summary, we prepared APS-modified $ZnIn_2S_4$ and investigated its photocatalytic hydrogen production performance. The introduction of silane alkyl chains increases steric hindrance and enhances the colloidal stability of the $ZnIn_2S_4$ suspension. The electron-donating $–NH_2$ broadens the light absorption of $ZnIn_2S_4$ and promotes the adsorption of H^+ on its surface. Under the synergistic effects of these factors, the photocatalytic performance and stability of $ZnIn_2S_4$ were significantly improved. The surface-modified ZIS-APS exhibited a photocatalytic H_2 evolution rate of 5.13 mmol·g^{-1}·h^{-1}, which was 1.46 times greater than that of pure ZIS. This finding indicates that surface modification is a simple and efficient measure for enhancing the photocatalytic performance of semiconductors and can be used for other photocatalyst systems in addition to TiO_2 and ZIS.

Author Contributions: X.C.: Conceptualization, Methodology, Formal analysis, Validation, Data curation, Writing—original draft. B.L.: Resources, Writing—original draft. L.Y.: Funding acquisition, project administration, supervision. All authors have read and agreed to the published version of the manuscript.

Funding: The work was supported by the National Natural Science Foundation of China (11475017).

Data Availability Statement: The data will be made available upon request.

Conflicts of Interest: The authors declare that they have no known competing financial interests or personal relationships that could have appeared to influence the work reported in this paper.

References

1. Ipatieff, V.N.; Monroe, G.S.; Fischer, L.E. Low temperature hydrogen production. *Ind. Eng. Chem.* **1950**, *42*, 92–94. [CrossRef]
2. Fujishima, A.; Honda, K. Electrochemical photolysis of water at a semiconductor Electrode. *Nature* **1972**, *238*, 37–38. [CrossRef] [PubMed]
3. Zhang, M.; Shang, Q.; Wan, Y.; Cheng, Q.; Liao, G.; Pan, Z. Self-template synthesis of double-shell TiO_2@ ZiF-8 hollow nanospheres via Ssonocrystallization with enhanced photocatalytic activities in hydrogen generation. *Appl. Catal. B Environ.* **2019**, *241*, 149–158. [CrossRef]
4. Prakash, J.; Kumar, P.; Saxena, N.; Chen, Z.; Tyagi, A.; Zhang, G.; Sun, S. CdS Based 3D Nano/microarchitectures: Formation mechanism, tailoring of visible light activities and emerging applications in photocatalytic H_2 production, CO_2 reduction and organic pollutant degradation. *J. Mater. Chem. A* **2023**, *11*, 10015–10064. [CrossRef]
5. Singh, R.; Dutta, S. A review on H2 production through photocatalytic reactions using TiO2/TiO2-assisted catalysts. *Fuel* **2018**, *220*, 607–620. [CrossRef]
6. Xiao, M.; Luo, B.; Wang, S.; Wang, L. Solar energy conversion on g-C3N4 photocatalyst: Light harvesting, charge separation, and surface kinetics. *J. Energy Chem.* **2018**, *27*, 1111–1123. [CrossRef]
7. Gogoi, D.; Namdeo, A.; Golder, A.K.; Peela, N.R. Ag-doped TiO_2 photocatalysts with effective charge transfer for highly efficient hydrogen production through water splitting. *Int. J. Hydrogen Energy* **2020**, *45*, 2729–2744. [CrossRef]
8. Bi, R.; Han, B.; Shen, Y.; Liu, J.; Wang, Z. Enhancing photocatalytic overall water splitting activity of $SrTiO_3$ nanoparticles by a synergetic Pt/CrOx dual cocatalyst system. *ACS Appl. Energy Mater.* **2023**, *6*, 10600–10609. [CrossRef]
9. Zheng, Z.; Xie, W.; Huang, B.; Dai, Y. Plasmon-enhanced solar water splitting on metal semiconductor photocatalysts. *Chem.-A Eur. J.* **2018**, *24*, 18322–18333. [CrossRef]
10. Shi, R.; Ye, H.F.; Liang, F.; Wang, Z.; Li, K.; Weng, Y.; Lin, Z.; Fu, W.; Che, C.; Chen, Y. Interstitial P-doped CdS with long-lived photogenerated electrons for photocatalytic water splitting without sacrificial Agents. *Adv. Mater.* **2018**, *30*, 1705941. [CrossRef]
11. Jia, G.; Wang, Y.; Cui, X.; Zheng, W. Highly carbon-doped TiO_2 derived from mxene boosting the photocatalytic hydrogen evolution. *ACS Sustain. Chem. Eng.* **2018**, *6*, 13480–13486. [CrossRef]
12. Zhang, L.; Jing, D.; Guo, L.; Yao, X. In situ photochemical synthesis of Zn-doped Cu2O hollow microcubes for highly efficient photocatalytic H2 production. *ACS Sustain. Chem. Eng.* **2014**, *2*, 1446–1452. [CrossRef]
13. Sinhamahapatra, A.; Jeon, J.P.; Yu, J.S. A new approach to prepare highly active and stable black titania for visible light-assisted hydrogen production. *Energy Environ. Sci.* **2015**, *8*, 3539–3544. [CrossRef]
14. Bai, S.; Zhang, N.; Gao, C.; Xiong, Y. Defect engineering in photocatalytic materials. *Nano Energy* **2018**, *53*, 296–336. [CrossRef]
15. Ou, G.; Xu, Y.; Wen, B.; Lin, R.; Ge, B.; Tang, Y.; Liang, Y.; Yang, C.; Hang, K.; Zu, D. Tuning defects in oxides at room temperature by lithium reduction. *Nat. Commun.* **2018**, *9*, 1302. [CrossRef]
16. Guan, X.; Zhang, X.; Zhang, C.; Li, R.; Liu, J.; Wang, Y.; Fan, C.; Li, Z. Original self-assembled S-Scheme BiOBr-(001)/Bi_2SiO_5/Bi heterojunction photocatalyst with rich oxygen vacancy for boosting CO_2 reduction performance. *J. Colloid Interface Sci.* **2023**, *644*, 426–436. [CrossRef]
17. Gao, H.; Zhang, P.; Hu, J.; Pan, J.; Fan, J.; Shao, G. One-dimensional Z-scheme TiO_2/WO_3/Pt heterostructures for enhanced hydrogen generation. *Appl. Surf. Sci.* **2017**, *391*, 211–217. [CrossRef]
18. Shen, J.; Wang, R.; Liu, Q.; Yang, X.; Tang, H.; Yang, J. Accelerating photocatalytichydrogen evolution and pollutant degradation by coupling organic co-catalystswith TiO_2. *Chin. J. Catal.* **2019**, *40*, 380–389. [CrossRef]
19. Feng, C.; Wu, Z.P.; Huang, K.W.; Ye, J.; Zhang, H. surface modification of 2D photocatalysts for solar energy conversion. *Adv. Mater.* **2022**, *34*, 2200180. [CrossRef]
20. Lin, X.; Xu, S.; Wei, Z.Q.; Hou, S.; Xiao, F.X. Selective Organic Transformation over a Self-Assembled AllSolid-State Z-Scheme Core-Shell Photoredox System. *J. Mater. Chem. A* **2020**, *8*, 20151–20161. [CrossRef]
21. Wu, J.-W.; Wei, Y.C.; Torimoto, T.; Chien, Y.N.; Chen, C.Y.; Chang, T.M.; Sone, M.; Hsieh, P.Y.; Hsu, Y.I. Yolk@Shell Nanostructures for Water Splitting: Current Development and Future Prospects. *ACS Materials Lett.* **2024**, *6*, 4066–4089. [CrossRef]
22. Hu, J.; Xie, J.; Jia, W.; Zhang, S.; Cao, Y. Interesting molecule adsorption strategy induced energy band tuning: Boosts 43 times photocatalytic water splitting ability for commercial TiO_2. *Appl. Catal. B* **2020**, *268*, 118753. [CrossRef]
23. Wanag, A.; Sienkiewicz, A.; Rokicka-Konieczna, P.; Kusiak-Nejman, E.; Morawski, A.W. Influence of modification of titanium dioxide by silane coupling agents on the photocatalytic activity and stability. *J. Environ. Chem. Eng.* **2020**, *8*, 103917. [CrossRef]
24. Lei, W.; Wang, H.; Khan, S.; Suzuki, N.; Takagi, K.; Katsumata, K.; Teshima, K.; Terashima, C.; Fujishima, A. Interfacial molecular regulation of TiO_2 for enhanced and stable cocatalyst-free photocatalytic hydrogen production. *J. Colloid Interface Sci.* **2023**, *645*, 219–226. [CrossRef]
25. Shao, W.; Wang, L.; Wang, H.; Zhao, Z.; Xie, Y. Efficient exciton dissociation in heterojunction interface realizing enhanced photoresponsive performance. *J. Phys. Chem. Lett.* **2019**, *10*, 2904–2910. [CrossRef] [PubMed]

26. Chai, B.; Peng, T.; Zeng, P.; Zhang, X.; Liu, X. Template-free hydrothermal synthesis of $ZnIn_2S_4$ floriated microsphere as an efficient photocatalyst for H_2 production under visible-light irradiation. *J. Phys. Chem. C* **2011**, *115*, 6149–6155. [CrossRef]
27. Xue, C.; An, H.; Yan, X.; Li, J.; Yang, B.; Wei, J.; Yang, G. Spatial charge separation and transfer in ultrathin $CdIn_2S_4$/rGO nanosheet arrays decorated by ZnS quantum dots for efficient visible-light-driven hydrogen evolution. *Nano Energy* **2017**, *39*, 513–523. [CrossRef]
28. Yang, W.; Zhang, L.; Xie, J.; Zhang, X.; Liu, Q.; Yao, T.; Wei, S.; Zhang, Q.; Xie, Y. Enhanced photoexcited carrier separation in oxygen-doped $ZnIn_2S_4$ nanosheets for hydrogen evolution. *Angew. Chem. Int. Ed.* **2016**, *55*, 6716–6720. [CrossRef]
29. Yu, M.S.; Lv, X.Y.; Idris, A.M.; Li, S.H.; Lin, J.Q.; Lin, H.; Wang, J.; Li, Z.Q. Upconversion nanoparticles coupled with hierarchical $ZnIn_2S_4$ nanorods as a near-infrared responsive photocatalyst for photocatalytic CO_2 reduction. *J. Colloid. Interf. Sci.* **2022**, *612*, 782–791. [CrossRef]
30. Sun, L.L.; Liu, X.S.; Jiang, X.H.; Feng, Y.B.; Ding, X.L.; Jiang, N.; Wang, J.G. An internal electric field and interfacial S–C bonds jointly accelerate S-scheme charge transfer achieving efficient sunlight-driven photocatalysis. *J. Mater. Chem. A* **2022**, *10*, 25279–25294. [CrossRef]
31. Chen, H.; Wu, J.; Zhu, Y.; Yang, J.; Tang, B.; Zhang, T.; Yang, H. Cu-MOF modified $ZnIn_2S_4$ nanosheet composite catalyst for photocatalytic hydrogen production. *Renew. Energy* **2024**, *228*, 120672. [CrossRef]
32. Zhang, H.; Cui, M.; Lv, Y.; Rao, Y.; Huang, Y. A short review on research progress of $ZnIn_2S_4$-based S-scheme heterojunction:Improvement strategies. *Chin. Chem. Lett.* 2024, *in press*. [CrossRef]
33. Zhang, Y.; Chen, D.; Li, N.; Xu, Q.; Li, H.; Lu, J. Fabricating 1D/2D $Co_3O_4/ZnIn_2S_4$ core–shell heterostructures with boosted charge transfer for photocatalytic hydrogen production. *Appl. Surf. Sci.* **2023**, *610*, 155272. [CrossRef]
34. Cai, X.; Zang, Y.; Zang, S.; Tang, S.; Jing, F.; Mo, L.; Teng, D.; Lin, W.; Zhang, G. Binary pyrene-benzene polymer/Znln2S4 S-scheme photocatalyst for enhanced hydrogen evolution and antibiotics degradation. *Appl. Surf. Sci.* **2023**, *637*, 157871. [CrossRef]
35. Xu, Q.L.; Zhang, L.Y.; Cheng, B.; Fan, J.; Yu, J. S-Scheme Heterojunction Photocatalyst. *Chem* **2020**, *6*, 1543–1559. [CrossRef]
36. Chai, S.Y.; Kim, Y.J.; Jung, M.H.; Chakraborty, A.K.; Jung, D.; Wang, I.L. Heterojunctioned $BiOCl/Bi_2O_3$, a new visible light photocatalyst. *J. Catal.* **2009**, *262*, 144–149. [CrossRef]
37. Kumar, Y.; Sudhaik, A.; Sharma, K.; Sonu; Raizada, P.; Khan, A.A.P.; Nguyen, Y.H.; Ahamad, T.; Singh, P.; Asiri, A.M. Construction of magnetically separable novel arrow down dual S-scheme $ZnIn_2S_4/BiOCl/FeVO_4$ heterojunction for improved photocatalytic activity. *J. Photochem. Photobiol. A Chem.* **2023**, *435*, 114326. [CrossRef]
38. Liu, X.T.; Jiang, Z.J.; Cao, X.; Shen, Z.; Zhao, W.; Wanf, F.; Cui, M.; Liang, C. Fabrication of S-scheme g-C3N4/$Zn_4In_2S_7$ heterojunction photocatalyst for enhancing selective cleavage of β-O-4 bond in lignin model compounds and lignin. *ACS Sustain. Chem. Eng.* **2023**, *11*, 14947–14959. [CrossRef]
39. Wang, Y.J.; Sun, L.L.; Li, X.L. Ultrasonic-assistant hydrothermal synthesis of $ZnIn_2S_4$/graphene-quantum-dots nanowires and the sono-effect improved catalytic activity. *J. Water Process Eng.* **2024**, *65*, 105807. [CrossRef]
40. Demir, R.; Göde, F.; Güneri, E.; Mehmet, E.F. The effect of nanoparticle sizes on the structural, optical and electrical properties of indium sulfide thin films consisting of In_2S_3 and In_6S_7 phases. *J. Mol. Struct.* **2021**, *1227*, 129565. [CrossRef]
41. Duan, S.; Li, A.; Wang, Y.; Chen, X.; Liu, B.; Liang, B.; Dai, C.; Yan, L.; Guo, J. Fabrication and performance of a 3D porous graphene aerogel-supported Ni–ZnS composite photocatalyst. *Colloids Surf. A Physicochem. Eng. Asp.* **2024**, *682*, 132948. [CrossRef]
42. Huang, W.X.; Li, Z.P.; Wu, C.; Zhang, H.J.; Sun, J.; Lin, Q. Delaminating Ti_3C_2 MXene by blossom of $ZnIn_2S_4$ microflowers for noble-metal-free photocatalytic hydrogen production. *J. Mater. Sci. Technol.* **2022**, *120*, 89–98. [CrossRef]
43. Zhao, M.Y.; Liu, S.; Chen, D.M.; Zhang, S.S.; Carabineiro, S.A.C.; Lv, K.L. A novel S-scheme 3D $ZnIn_2S_4/WO_3$ heterostructure for improved hydrogen production under visible light irradiation. *Chin. J. Catal.* **2022**, *43*, 2615–2624. [CrossRef]
44. Zhou, D.X. $ZnIn_2S_4$ Photocatalysts: Structural Design, Controllable Preparation and Their Photocatalytic Hydrogen Evolution Performance. Ph.D. Thesis, Beijing University of Science and Technology, Beijing, China, 2022.
45. Yuan, Y.J.; Tu, J.R.; Ye, Z.J.; Chen, D.Q.; Hu, B.; Huang, Y.W.; Chen, T.T.; Cao, D.P.; Yu, Z.T.; Zou, Z.G. MoS_2-graphene/$ZnIn_2S_4$ hierarchical microarchitectures with an electron transport bridge between light-harvesting semiconductor and cocatalyst: A highly efficient photocatalyst for solar hydrogen generation. *Appl. Catal. B Environ.* **2016**, *188*, 13–22. [CrossRef]
46. Wang, L.F.; Zeng, Q.R.; Gan, Y.F.; Wei, Y.Z.; Wang, X.P.; Zeng, D.Q. Insight into the role of nickel carbide nanoparticles in improving photocatalytic H_2 generation over $ZnIn_2S_4$ under visible light. *FlatChem* **2024**, *47*, 100711. [CrossRef]
47. Ji, M.X.; Wen, J.; Xu, Q.Y. Highly efficient visible-light-driven water splitting for H_2 evolution and degradation of ECs using $CdS/ZnIn_2S_4$ S-scheme heterojunction with built-in electric field. *Fuel* **2024**, *374*, 132444. [CrossRef]
48. Du, C.; Zhang, Q.; Lin, Z.Y.; Yan, B.; Xia, C.X.; Yang, G.W. Half-unit-cell $ZnIn_2S_4$ monolayer with sulfur vacancies for photocatalytic hydrogen evolution. *Appl. Catal. B Environ.* **2019**, *248*, 193–201. [CrossRef]